Acta Crystallographica Section D
Biological Crystallography
ISSN 0907-4449

1.8 and 1.9 Å resolution structures of the *Penicillium amagasakiense* and *Aspergillus niger* glucose oxidases as a basis for modelling substrate complexes

Gerd Wohlfahrt,[a]† Susanne Witt,[a]‡ Jörg Hendle,[b]§ Dietmar Schomburg,[b]† Henryk M. Kalisz[a] and Hans-Jürgen Hecht[b]*

[a]Department of Enzymology, GBF – Gesellschaft für Biotechnologische Forschung mbH, Mascheroder Weg 1, D-38124 Braunschweig, Germany, and [b]Department of Molecular Structure Research, GBF – Gesellschaft für Biotechnologische Forschung mbH, Mascheroder Weg 1, D-38124 Braunschweig, Germany

† Present address: Universität zu Köln, Institut für Biochemie, Zülpicher Str. 47, D-50674 Köln, Germany.
‡ Present address: Department of Biochemistry, Arrhenius Laboratories for Natural Sciences, Stockholm University, S-10691 Stockholm, Sweden.
§ Present address: EMBL Outstation, Hamburg, Germany.

Correspondence e-mail: hjh@gbf.de

Received 25 November 1998
Accepted 2 March 1999

PDB Reference: glucose oxidase (*A. niger*), 1cf3; glucose oxidase (*P. amagasakiense*), 1gpe.

Glucose oxidase is a flavin-dependent enzyme which catalyses the oxidation of β-D-glucose by molecular oxygen to δ-gluconolactone and hydrogen peroxide. The structure of the enzyme from *Aspergillus niger*, previously refined at 2.3 Å resolution, has been refined at 1.9 Å resolution to an *R* value of 19.0%, and the structure of the enzyme from *Penicillium amagasakiense*, which has 65% sequence identity, has been determined by molecular replacement and refined at 1.8 Å resolution to an *R* value of 16.4%. The structures of the partially deglycosylated enzymes have an r.m.s. deviation of 0.7 Å for main-chain atoms and show four *N*-glycosylation sites, with an extended carbohydrate moiety at Asn89. Substrate complexes of the enzyme from *A. niger* were modelled by force-field methods. The resulting model is consistent with results from site-directed mutagenesis experiments and shows the β-D-glucose molecule in the active site of glucose oxidase, stabilized by 12 hydrogen bonds and by hydrophobic contacts to three neighbouring aromatic residues and to flavin adenine dinucleotide. Other hexoses, such as α-D-glucose, mannose and galactose, which are poor substrates for the enzyme, and 2-deoxy-D-glucose, form either fewer bonds or unfavourable contacts with neighbouring amino acids. Simulation of the complex between the reduced enzyme and the product, δ-gluconolactone, has provided an explanation for the lack of product inhibition by the lactone.

1. Introduction

Glucose oxidase (GOX; β-D-glucose:oxygen 1-oxidoreductase, E.C. 1.1.3.4) is a flavoprotein which catalyses the oxidation of β-D-glucose by molecular oxygen to δ-gluconolactone and hydrogen peroxide. Glucose oxidase activity has been identified from various sources, but most of the biochemical characterization has been carried out with the enzyme from *Aspergillus niger*. GOX is of considerable commercial importance, with the enzymes from *A. niger* and *Penicillium amagasakiense* being used commercially, mostly in biosensors (Wilson & Turner, 1992). They are homodimeric glycoproteins of molecular weight 160 kDa, with one tightly but noncovalently bound flavin adenine dinucleotide (FAD) cofactor per monomer.

The two GOXs show an 81% sequence similarity (blosum62 matrix; Kiess *et al.*, 1998) and exhibit similar glucose oxidation kinetics, although the *P. amagasakiense* GOX has a sixfold higher affinity constant (corresponding to lower K_m) for β-D-glucose and a tenfold higher specificity constant (k_{cat}/K_m) than its *A. niger* counterpart (Kalisz *et al.*, 1997). The catalytic cycle can be separated, as for other flavoenzymes, into two half-reactions. The reductive half-reaction (Fig. 1) of GOX

involves the oxidation of β-D-glucose to δ-gluconolactone by hydride transfer to the flavin system, probably initiated by proton abstraction from the glucose O1 hydroxyl group. The product δ-gluconolactone is subsequently hydrolysed non-enzymatically to gluconic acid. In the oxidative half-reaction, two protons and two electrons are transferred from the enzyme to molecular oxygen, yielding hydrogen peroxide and regenerating the oxidized state of the enzyme. A mechanism for the whole reaction with individual rate constants in a pH-dependent scheme (Bright & Appleby, 1969) has been proposed from a number of steady-state and transient-state kinetic analyses (for a review, see Bright & Porter, 1975).

GOX from *A. niger* and *P. amagasakiense* is highly specific for β-D-glucose, having at least a fivefold higher turnover rate (k_{cat}) and, with the exception of 2-deoxy-D-glucose, at least a 20-fold higher affinity than for other monosaccharides (Pazur & Kleppe, 1964). The specificity constant (k_{cat}/K_m) for β-D-glucose is therefore at least 30 times higher than for other sugars. A molecular interpretation of the high substrate specificity of GOX has been hampered by the absence of experimentally determined structures of enzyme–substrate complexes. In this study, we refined the X-ray structures of the enzyme from *A. niger* (asp-gox) and *P. amagasakiense* (pen-gox) to high resolution and carried out computational studies of enzyme–substrate and enzyme–product complexes of asp-gox in order to obtain information about the role of individual enzyme residues and of the cofactor FAD in the high substrate specificity and lack of product inhibition.

2. Materials and methods

2.1. Purification and crystallization

Commercially available glucose oxidase from *P. amagasakiense* (Nagase, Osaka, Japan) was purified by gel filtration and anion-exchange chromatography, partially deglycosylated with endoglycosidase H and repurified by gel filtration (Hendle *et al.*, 1992). The enzyme crystallizes from 1.3 *M* ammonium sulfate, 100 m*M* citrate–phosphate buffer pH 7.4 in the orthorhombic space group $P2_12_12_1$, with unit-cell dimensions a = 57.6, b = 132.1, c = 151.3 Å and one dimeric molecule per asymmetric unit. The enzyme from *A. niger* was purified, partially deglycosylated and crystallized as described previously (Kalisz *et al.*, 1990). The refined unit-cell dimensions for the trigonal space group $P3_121$ are a = 67.5, c = 215.4 Å; the asymmetric unit contains one monomer.

2.2. Structure determination and refinement

The structure of the enzyme from *P. amagasakiense* was solved by molecular replacement with *MERLOT* (Fitzgerald, 1988) using the partially refined coordinates of *A. niger* GOX (Hecht *et al.*, 1993) and a 2.5 Å data set collected on a Rigaku rotating-anode generator using Cu $K\alpha$ radiation. Rigid-body refinement, energy minimization and simulated annealing with *X-PLOR* (Brünger *et al.*, 1987) reduced the R value from 52.1 to 35.0% for a partial model consisting of 552 alanine residues. At this stage, the sequence information for the enzyme was incomplete, and the subsequent refinement was therefore based on the known fragments from the pen-gox sequence interspersed with parts of the asp-gox sequence. The model was completed by several cycles of manual rebuilding with *FRODO* (Jones, 1985) and energy refinement and simulated annealing with *X-PLOR*. The final R value at this stage was 17.7% for 8.0–2.5 Å data and a model consisting of 582 residues, one FAD cofactor, four *N*-acetylglucosamine molecules and 237 water molecules. The high-resolution data sets for pen-gox and asp-gox were collected at beamline BW6 at DESY with a wavelength of 1.0 Å. Both data sets were processed with *DENZO* (Otwinowski & Minor, 1996) and their statistics are given in Table 1. The pen-gox refinement started with the earlier model corrected for the now complete sequence (Kiess *et al.*, 1998); for asp-gox, the coordinates refined at 2.35 Å (PDB code 1gal) were used. The resolution was increased to 1.8 and 1.9 Å, respectively, by several cycles of energy minimization with *X-PLOR* and manual correction of the model with *O* (Jones *et al.*, 1991) and *XtalView* (McRee, 1993). During this stage, the strict non-crystallographic symmetry for pen-gox was relaxed to non-crystallographic symmetry restraints, resulting in a decrease in the conventional and free R values by 4.7 and 4.5%, respectively. In both cases, the final refinement was carried out with *REFMAC* (Collaborative Computational Project, Number 4, 1994). The non-crystallographic symmetry restraints for pen-gox were dropped at this stage owing to the presence of several different side-

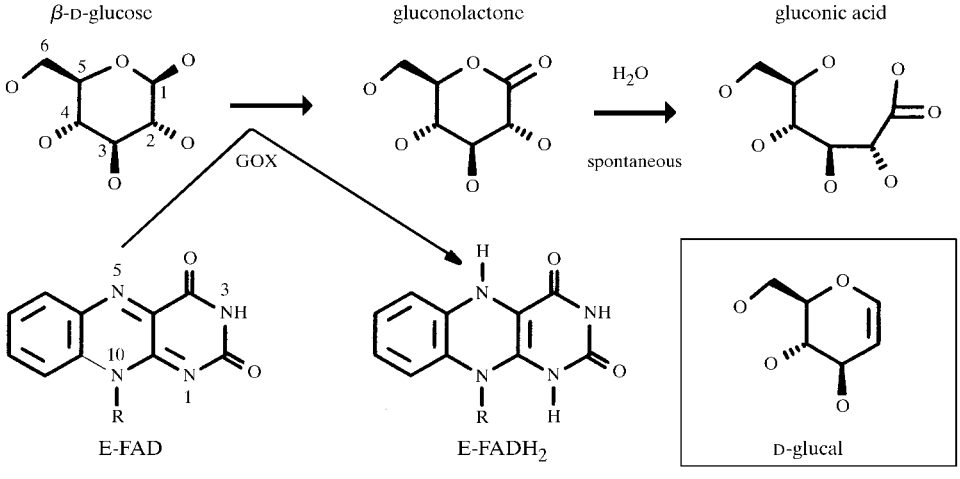

Figure 1
Schematic representation of the glucose oxidase reaction showing the inhibitor D-glucal in the insert. For β-D-glucose and the flavin group the atom-numbering scheme used in the text is indicated. Gluconolactone, gluconic acid and the inhibitor D-glucal are numbered accordingly.

Table 1
Data set and refinement statistics.

	Asp-gox†	Pen-gox‡
Space group	$P3_121$	$P2_12_12_1$
Unit-cell parameters		
a (Å)	67.5	57.6
b (Å)	67.5	132.1
c (Å)	215.4	151.3
Resolution range (Å)	20.0–1.9	20.0–1.8
Unique reflections	40401	101999
Completeness (%)	87.7 (78.7)	94.7 (90.0)
$\langle I/(I)\rangle$	21.5 (6.9)	18.4 (8.5)
$R_{\rm merge}$§ (%)	5.4 (12.2)	6.8 (13.2)
Refinement		
$R_{\rm all}$¶ (%)	19.0 (24.2)	16.4 (17.9)
$R_{\rm free}$ (%)	24.3 (32.9)	19.8 (23.7)
Bond distance r.m.s.d. (Å)	0.008	0.008
Angle distance r.m.s.d. (Å)	0.023	0.028
Plane r.m.s.d. (Å)	0.099	0.108
$\langle B\rangle$, protein atoms (Å^2)	23.3	13.8
$\langle B\rangle$, solvent atoms (Å^2)	33.7	24.9

† Data in parentheses refer to the highest resolution shell (1.99–1.90 Å). ‡ Data in parentheses refer to the highest resolution shell (1.88–1.80 Å). § $R_{\rm merge} = [\sum I_i(hkl) - \langle I(hkl)\rangle)]/\sum I_i(hkl)$. ¶ $R_{\rm all} = [\sum |F_o(hkl) - F_c(hkl)|]/\sum F_o(hkl)$.

chain conformations in the two dimer subunits. The final R values for pen-gox and asp-gox are 16.4% for 20.0–1.8 Å data and 9.0% for 20.0–1.9 Å data, respectively.

2.3. Modelling of enzyme–substrate complexes

The protein-modelling package *BRAGI* (Schomburg & Reichelt, 1988) and the molecular-mechanics program *AMBER* 4.0 (Pearlman *et al.*, 1991) were used for the simulation of enzyme–substrate complexes. The *AMBER* all-atom force field (Cornell *et al.*, 1995) was used with additional parameters for the saccharide, lactone and FAD derivatives. The parameters were fitted to reproduce the experimental data from these molecules and some smaller model compounds (Wohlfahrt, unpublished work). The molecular electrostatic potentials were derived from *ab initio* calculations with *GAUSSIAN* 94 (Frisch *et al.*, 1995) at the B3LYP/6-31G* level (Lee *et al.*, 1988; Becke, 1993; Hehre *et al.*, 1972; Hariharan & Pople, 1973). A two-stage restrained electrostatic potential fit method (RESP) was used to obtain atomic point charges (Bayly *et al.*, 1993; Cornell *et al.*, 1993).

All calculations were based on the refined X-ray structure of asp-gox. Histidines were assumed to be protonated at both N atoms in accordance with the overall charge determination (Voet *et al.*, 1981), with the exception of the active-site histidines whose protonation state was changed in some calculations. Substrate molecules were docked manually into the substrate-binding pocket, equilibrated by molecular dynamics and energy minimized. The force-field calculations were carried out with explicit TIP3P water molecules (Jorgensen *et al.*, 1983) at a dielectric constant $\varepsilon = 1$. A cutoff distance of 8 Å for the non-bonded interactions was used. During the molecular-dynamics simulations, the *SHAKE* algorithm (Ryckaert *et al.*, 1977) was used to constrain the covalent bonds to their equilibrium bond length. 15 crystallographic water molecules from the active-site region were added to the system and the *AMBER EDIT* program was used to fill the space within a 10 Å radius of the N5 of isoalloxazine. The water molecules were constrained to the centre of the sphere by a harmonic potential with a force constant of 2.1 kJ Å^{-2}. Only the atoms of the residues inside the 10 Å radius were allowed to move during these simulations. The structures were energy-minimized and then equilibrated by molecular dynamics for 100 ps at 298 K with an integration interval of 1 fs. The resulting structures were again energy-minimized and analysed for their similarity to the X-ray structure and their energetic and geometric properties.

3. Results and discussion

3.1. Quality of the structures

The final R value for pen-gox is 16.4% for 20.0–1.8 Å data with a model consisting of 587 residues, one FAD cofactor, five *N*-acetylglucosamine molecules and three mannose molecules per monomer together with 709 solvent molecules. The r.m.s. coordinate error, calculated with *SIGMAA* (Collaborative Computational Project, Number 4, 1994) is 0.09 Å. The r.m.s. displacement between the two molecules of the asymmetric unit, which were independently refined in the final refinement stage, is 0.3 Å for all protein atoms. The electron density is weak at the last C-terminal residue and conformational differences between the two molecules of the asymmetric unit indicate flexibility of the first five N-terminal residues. 89.0% of all residues occupy the core regions of a Ramachandran plot calculated with *PROCHECK* (Laskowski *et al.*, 1993; Collaborative Computational Project, Number 4, 1994). The sole residue in a generously-allowed region of the Ramachandran plot is Thr417, which is situated in a β-hairpin loop and shows very good electron density.

For asp-gox, the R value is 19.0% for 20.0–1.9 Å data and a model consisting of 581 residues, one FAD cofactor, five *N*-acetylglucosamine molecules, three mannose molecules and 309 solvent molecules. Electron density is not visible for the first two N-terminal residues and is weak (real-space correlation coefficient below 0.85) at the flexible surface loop 256–260 and at the last two C-terminal residues. The r.m.s. coordinate error calculated with *SIGMAA* is 0.2 Å, and 88.6% of all residues occupy the core regions of a Ramachandran plot calculated with *PROCHECK*. In asp-gox, Thr417 is again the sole residue in the generously allowed region of the Ramachandran plot, and again shows very good electron density. The r.m.s. difference to the earlier model (Hecht *et al.*, 1993; PDB code 1gal, refined at 2.35 Å) is 0.38 Å for main-chain atoms and 0.72 Å for all protein atoms. Deviations larger than two r.m.s.d. occur for main-chain atoms at the N- and C-terminal residues Gly3 and Met582–Gln583, which have weak electron density, at the flexible loop 256–262, which has improved electron density in the high-resolution refinement, and at Lys 273–Gly 274, where a different conformation of the main chain (peptide flip) was apparent.

3.2. Comparison of the structures

Pen-gox has an 81% sequence homology (blosum62 matrix) and a 65% identity (Kiess *et al.*, 1998) to asp-gox, with a one-residue deletion at asp-gox 87 and an N-terminal extension of five residues. The overall topology of pen-gox (Fig. 2) is identical to asp-gox, with structural differences larger than 3.0 Å for main-chain atoms occurring only at the N-terminus and at two loop regions in the vicinity of residues 260 and 312. For the monomer subunit, the r.m.s. difference to the main-chain atoms of asp-gox, as calculated with *LSQKAB* (Collaborative Computational Project, Number 4, 1994), is 0.74 Å when the residues corresponding to asp-gox 3, 87, 256–260 and 311–312 are excluded. Residue numbering for pen-gox will be based on the asp-gox numbering in the following text.

From the sequence of asp-gox, eight potential *N*-glycosylation sites can be identified. Four of these sites, Asn89, Asn161, Asn355 and Asn388, show clearly identifiable electron density for the *N*-acetylglucosamine moiety remaining after the deglycosylation procedure (Kalisz *et al.*, 1991). The fifth glycosylation site identified in 1gal, Asn168, shows some residual electron density in the higher resolution study, which may indicate a low-occupancy second conformation for the asparagine side chain together with an attached *N*-acetylglucosamine. This glycosylation site has not been included in the present asp-gox model. The higher resolution study confirms (with well resolved electron density) the extended carbohydrate structure at Asn89, consisting of a second *N*-acetylglucosamine and three mannose molecules. In the pen-gox sequence, seven of the eight potential glycosylation sites of asp-gox are conserved. The four sites corresponding to the confirmed asp-gox glycosylation sites also show well resolved electron density for the remaining *N*-acetylglucosamine in pen-gox, whereas the non-conserved sites do not appear to be glycosylated in either structure. The site corresponding to asp-gox Asn168 does not seem to be glycosylated, although peptide sequencing and ESI-MS analysis have shown this residue to probably contain a covalently linked *N*-acetylglucosamine (Kiess *et al.*, 1998). An extended carbohydrate structure very similar to asp-gox is also visible in pen-gox at the site corresponding to Asn89. This carbohydrate moiety forms a bridge between the two molecules of the dimer in both structures, with the second *N*-acetylglucosamine covering a small pocket formed by the conserved *cis*-Pro490–Gly491 motif. It contributes to a large extent to the surface becoming buried during dimer formation. The reduction of the accessible surface (Nicholls, 1993) per monomer is 1129 Å^2 neglecting the carbohydrate and 1789 Å^2, or 8.2% of the total surface, using all atoms. For pen-gox, the corresponding values are 1193 Å^2, 1928 Å^2 and 9.3%. In asp-gox, the dimer is stabilized further by six salt bridges and 15 hydrogen bonds, eight of them to the carbohydrate moiety. The salt bridges are not conserved in pen-gox, which only has two different salt bridges in the dimer interface but has 28 hydrogen bonds directly connecting the dimer, 15 of them to the carbohydrate. A superposition of the asp-gox and pen-gox dimers shows that the subunits in pen-gox are approximately 2.0 Å closer to each other as a consequence of these differences in the dimer contacts.

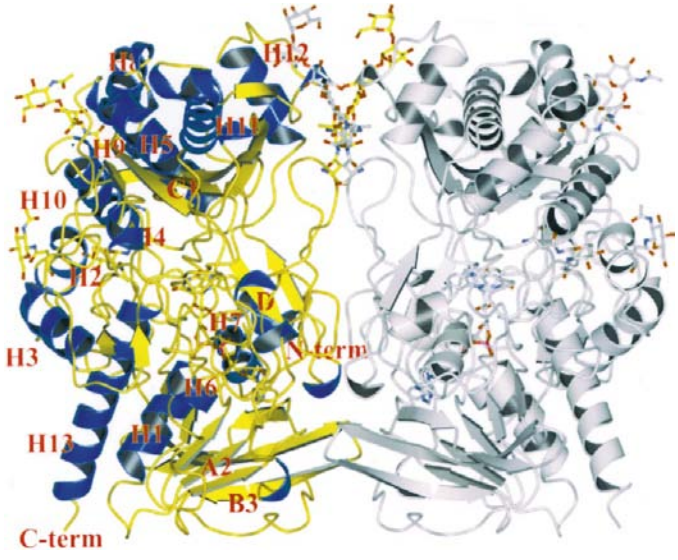

Figure 2
Ribbon diagram of glucose oxidase from *P. amagasakiense* with the attached carbohydrate and the cofactor FAD, drawn with *MOLSCRIPT* (Kraulis, 1991) and rendered with *gl_render* (Esser & Deisenhofer, unpublished program) and *POV-Ray*. Helices and β-sheets are labelled in one subunit; the second subunit of the dimer is coloured grey.

Asn89, with the extended carbohydrate moiety, is situated at the tip of a lid with the irregular two-stranded antiparallel β-sheet structure formed by residues 75–98. The lid covers the ribose part of the FAD cofactor and is mostly buried in the dimer interface, thus preventing release of the cofactor from the dimer. The deletion at residue 85 causes only a local distortion of the turn connecting the strands, but leaves the position of the glycosylated Asn89 almost identical to asp-gox. The distortion of the lid from a regular β-sheet is probably caused by the conserved Thr82, which forms hydrogen bonds from the side-chain O$^{\gamma}$ to the backbone carbonyl O atom of the conserved Val83 and to the backbone N atom of either Ala92 in asp-gox or Asn92 in pen-gox.

11 and 16 intramolecular salt bridges are formed in the asp-gox and pen-gox monomers, respectively. Five of these salt bridges are common to both structures. Three of these are located in the FAD-binding domain, where Arg545 on strand A5 of β-sheet A is connected by salt bridges to Glu284 on strand A4 and to Asp578 on the C-terminal helix H13; the third salt bridge connects Arg37 with Glu40, both on helix H1. The remaining two conserved salt bridges are located in the substrate-binding domain. The first connects helix H11 at the back of the substrate-binding β-sheet C *via* Arg472 with Glu487 on strand C6. The second involves the flavin-attachment loop formed by residues 106–114 and carrying Asn107, which contacts the *si*-face of the flavin system. Arg113 connects the C-terminal end of this loop with Glu144 at the C-terminus of helix H3 on the surface and contributes to an extensive hydrogen-bond network which includes the side chains of Trp111, Glu144, His165, Asp203 and Glu487. The area is further stabilized by the conserved disulfide bridge

Cys164–Cys206. In pen-gox, the hydrogen-bond network is slightly altered owing to the exchange of Gly205 for Leu, and Glu144 is only connected indirectly to His165 *via* a water molecule. A path for electron transfer from the flavin cofactor to the surface of the protein has been proposed passing through this area from the flavin O4 *via* Thr110, Trp111, Glu144 and His165 to Cys164 (Alvarez-Icaza *et al.*, 1995).

The FAD-binding site in pen-gox is almost identical to that in asp-gox. With the exception of His78 and Thr110, all residues forming hydrogen bonds to the cofactor are conserved. The hydrogen bond connecting His78 $N^{\varepsilon 2}$ at the base of the lid with the ribose O2′ of the FAD cofactor in asp-gox is replaced by a corresponding hydrogen bond of Gln78 $N^{\varepsilon 2}$ in pen-gox. The exchange of Thr110 for Ser110 in pen-gox conserves the side-chain hydrogen bond to the flavin O4. In both structures, the flavin O4 is also connected by hydrogen bonds to the backbone N atoms of Thr/Ser110 (asp-gox 3.2 Å, pen-gox 3.0 Å) and Gly108 (asp-gox 3.5 Å, pen-gox 3.3 Å). Similar backbone hydrogen bonds to this structurally highly conserved loop covering the *si*-face of the flavin moiety are also found in the related cholesterol oxidase (Vrielink *et al.*, 1991; Li *et al.*, 1993). Residues of the active site in front of the flavin system are conserved in asp-gox and pen-gox with the exception of Tyr515. This is replaced in pen-gox by Trp515, which forms very similar hydrophobic contacts to the flavin dimethyl side. The similarity of the active sites extends to five water molecules located at almost identical positions in both structures (Fig. 3).

Pen-gox and asp-gox both have two histidines in the active site, His516 and His559, which could act in the reaction scheme as general bases in the reductive half-reaction and as general acids in the oxidative half-reaction. His559 has a strong hydrogen bond at $N^{\varepsilon 2}$ to Glu412 $O^{\varepsilon 2}$ (asp-gox 2.6 Å, pen-gox 2.5 Å) and was proposed for this role because of this activation (Hecht *et al.*, 1993). This histidine is not conserved in cholesterol oxidase (Li *et al.*, 1993) and in other members of the glucose–methanol–choline (GMC) oxidoreductase family (Cavener, 1992), which show overall topological similiarity in a structure-based sequence alignment (Kiess *et al.*, 1998) and most probably have a similar reaction mechanism. His516, however, is conserved in all members of this family and has therefore been identified as the general base, although in the complex of cholesterol oxidase with the substrate analogue dehydroisoandrosterone its action is mediated by a water molecule (Li *et al.*, 1993).

3.3. Modelling of the enzyme–substrate complexes

3.3.1. The free oxidized enzyme. The X-ray structures of GOXs represent the state of the free oxidized enzyme. The side-chain conformations in the active sites are identical in both structures, with the exception of His516, which had been classified as flexible in the lower resolution study (Hecht *et al.*, 1993). In pen-gox, His516 forms hydrogen bonds at $N^{\delta 1}$ to the backbone carbonyl group of Asn514 and at $N^{\varepsilon 2}$ to the water molecule W481, which is situated in front of the flavin system. In asp-gox, the imidazolium group is rotated by 90° and His516 $N^{\delta 1}$ is hydrogen bonded to the carboxamide O atom of Gln329 (Fig. 3). His516 $N^{\varepsilon 2}$ again forms a hydrogen bond to the water molecule W110, which occupies almost the same position as W481 in pen-gox. Force-field calculations were carried out for both side-chain conformations with singly and doubly protonated histidines. They show that the conformation observed in pen-gox is unstable for His516 protonated on both N atoms owing to short contacts of the $N^{\varepsilon 2}$ hydrogen to the flavin ring, and is changed to the asp-gox conformation. However, this conformation is compatible with singly and doubly protonated histidine according to force-field calculations. Residual electron density in the vicinity of His516 suggests that a conformation similar to asp-gox may also be present in the pen-gox structure but with low occupancy. As pen-gox, which crystallized at pH 7.4 (away from the activity pH optimum), gives indications for both side-chain conformations, whereas asp-gox, which crystallized at pH 5.6 (near to the activity pH optimum), clearly shows only one side-chain conformation, the latter was used as a basis for subsequent modelling calculations.

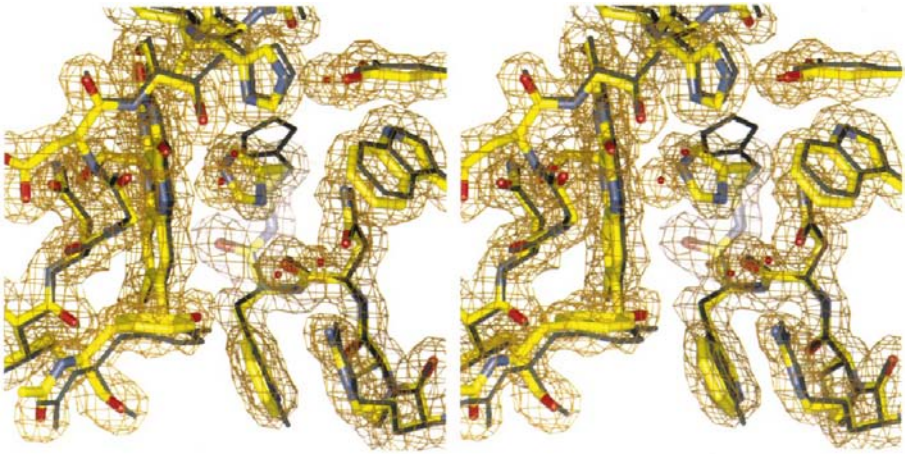

Figure 3
Active site of glucose oxidase from *P. amagasakiense*, drawn with *BOBSCRIPT* (Esnouf, 1997) and rendered with *gl_render* (Esser & Deisenhofer, unpublished program) and *POV-Ray*. The $2F_o - F_c$ electron density is contoured at 1 r.m.s.d. from mean density. Superposed residues of glucose oxidase from *A. niger* are coloured grey.

In both structures, His559 forms strong hydrogen bonds to Glu412 and to the water molecule W110/W481 in front of the flavin ring. Owing to the activation by Glu412, a doubly protonated state is most probable for this histidine over a broad pH range. The water molecule W110/W481, therefore, acts in all cases as a hydrogen acceptor for His559 $N^{\delta 1}$ (2.7 Å) and as a donor to pen-gox His516 $N^{\varepsilon 2}$ (2.8 Å); for asp-gox His516 $N^{\varepsilon 2}$ it may become a hydrogen acceptor at lower pH when His516 is doubly protonated.

3.3.2. The substrate/product-complex models. In the absence of

crystallographic data for enzyme–substrate complexes, modelling calculations were performed in order to provide an insight into the most probable position of β-D-glucose in the active site of GOX. A β-D-glucose molecule (start coordinates from the *ab initio* optimization with the B3LYP/6-31G* basis) was placed manually in the active site of asp-gox, from which three crystallographic water molecules had been removed, and a series of different orientations relative to the enzyme and cofactor were energy minimized by force-field calculations. For all of these starting orientations, the basic assumption was made that the reacting CH group should be close to the isoalloxazine moiety, and the H atoms at C1 and O1 of glucose are therefore directed towards the accessible acceptor atoms of FAD, His559 $N^{\delta1}$ and His516 $N^{\varepsilon2}$. The torsion angles of the exocyclic hydroxymethylene group C6/O6 of β-D-glucose were also varied in this series. The resulting lowest energy complex is stable in the 100 ps MD simulation (Fig. 4) and has only minor deviations from the X-ray structure, with the side chains of Tyr68 and His516 moving by about 1.1 Å from their original positions to adapt to the presence of the glucose molecule. In this model (Fig. 5), all hydroxyl groups of β-D-glucose, except OH2, act simultaneously as hydrogen donor and acceptor in highly specific hydrogen bonds (Fig. 6) and the 1-, 3- and 6-hydroxyl groups occupy almost identical positions as the three crystallographic water molecules W110, W111 and W473 (W82, W481, W561 in pen-gox), which therefore may be regarded as anchors for the substrate in the X-ray structure. In addition to the 12 hydrogen bonds, the orientation of β-D-glucose in the active site is stabilized by hydrophobic contacts to Phe414, Trp426 and, to a lesser extent, Tyr68 and FAD.

In a parallel simulation, an attempt was made to simulate a complex with glucose in a manner similar to the complex found in cholesterol oxidase (Fig. 7; Li *et al.*, 1993), with the water molecule W110 kept in its observed position in the active site. Subsequent molecular-dynamics calculations, however, either led to the expulsion of this water molecule from the active site and its replacement by the glucose molecule, or to the formation of fewer and less specific contacts between glucose and the active-site residues when the water molecule was constrained to this position. These modelling calculations therefore suggest a direct interaction of the active histidine with the substrate in GOX and not a water-mediated interaction as in cholesterol oxidase.

In the present model complex, the glucose O1 hydroxyl group sits virtually equidistantly between His516 and His559, and a proton transfer to either one of these histidines would be sterically possible. In addition, the glucose molecule forms hydrogen bonds to Tyr68, Asn514, Arg512, His516, His559 and Thr/Ser110. Site-directed mutagenesis studies on GOX from *P. amagasakiense* (Witt, 1996) support this model. The wild-type enzyme has a binding constant K_m = 6.2 m*M* for glucose and this increases to 24.3 m*M* for the variant Tyr68Phe. The variant Asn514Thr has a similarly increased binding constant of 35.5 m*M*. This corresponds in both cases to the loss of one hydrogen bond in the model complex, from side chains of Tyr68 or Asn514 to the glucose, while the additional hydrogen bonds formed by the backbone carboxyl O atom of Asn514 to glucose can be maintained in the Asn514Thr variant. The contribution of Arg512 to the complex formation is emphasized by the variants Arg512Ala and Arg512Lys, which have K_m values

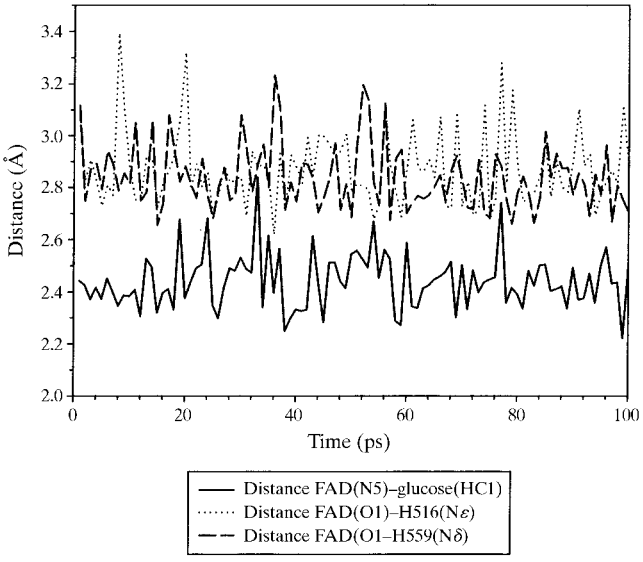

Figure 4
Plot of representative distances from the trajectory of a 100 ps MD simulation of the *A. niger* glucose oxidase complex with β-D-glucose indicating the stability of the complex [distance FAD(N5)–glucose(HC1)] and of the active-site residues [distances FAD(O1)–His516(N^{ε}) and FAD(O1)–His559(N^{δ})].

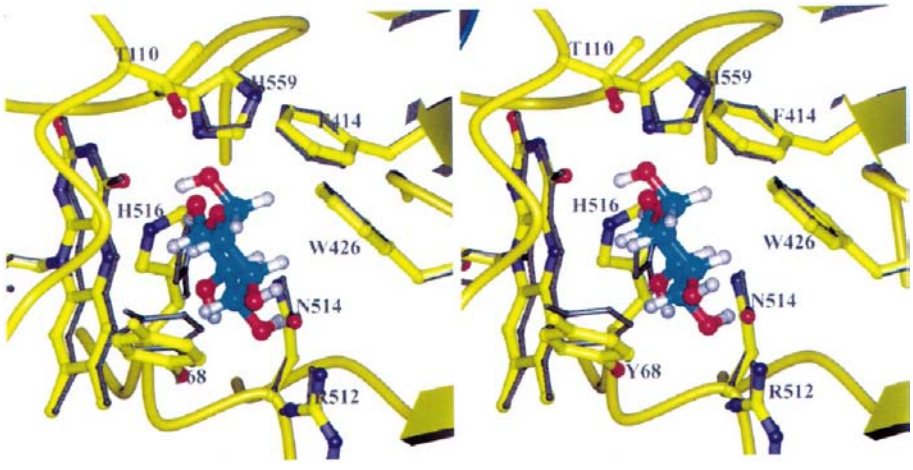

Figure 5
Stereoview of the active site of glucose oxidase from *A. niger* with the modelled substrate β-D-glucose, drawn with *MOLSCRIPT* (Kraulis, 1991) and rendered with *gl_render* (Esser & Deisenhofer, unpublished program) and *POV-Ray*. Residues of the energy-minimized model complex are shown in thin grey lines. For the glucose molecule, C atoms are coloured cyan and H atoms are coloured white.

of 1018.7 m*M* and 513.3 m*M*, respectively. Arg512 forms two side-chain hydrogen bonds to the glucose O3 and one to O4 in the model complex which are lost in the alanine variant. In the lysine variant, these hydrogen bonds are either very weak (distances >3.4 Å) owing to the shorter side chain of lysine or are accompanied by a displacement of the glucose molecule which weakens other hydrogen bonds. The variants His516Val and His559Val both have less than 10^{-4} times the wild-type activity and their respective K_m values are therefore uncertain.

Although the structures of β-D-glucose and δ-gluconolactone are very similar, only a very weak inhibitory effect of the lactone has been observed (Gibson *et al.*, 1964). Simulation of a complex between the reduced enzyme and the lactone shows His559 $N^{\delta1}$ forming a hydrogen bond to FAD O4 and His516 $N^{\varepsilon2}$ interacting with the region around N1 of the isoalloxazine anion. The isoalloxazine H(N5) is forced out of the flavin plane towards the lactone by the increased sp^3 hybridization of N5 (Sanner *et al.*, 1991) and the proximity of the Gly108 amide H atom (FAD N5–Gly108 N, 3.5 Å) on the flavin *si*-side. This results in an unfavourable interaction between the lactone C1 and the H(N5) of isoalloxazine, which forces the product out of the active site, thereby explaining the low affinity for the lactone.

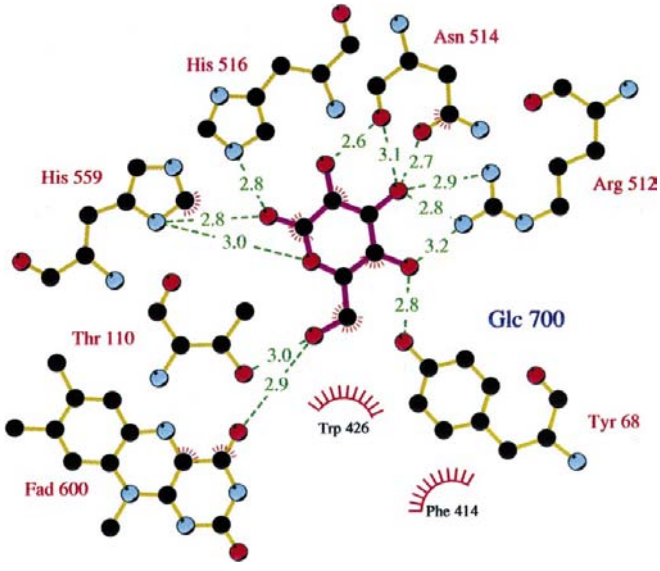

Figure 6
Schematic representation of the hydrogen bonds and hydrophobic interactions of the modelled substrate β-D-glucose with active-site residues in glucose oxidase from *A. niger* (*LIGPLOT*; Wallace *et al.*, 1995).

The competitive inhibitor D-glucal (Rogers & Brandt, 1971*a*; Fig. 7) can be modelled to an identical position to glucose in the active centre and this posititon remains virtually unchanged in 100 ps molecular-dynamics simulations with doubly protonated His516 and His559. D-Glucal, however, cannot be activated by proton abstraction for the reductive reaction step as it lacks the 1-hydroxy group of glucose. The reduced number of hydrogen bonds owing to this and the additional absence of the 2-hydroxy group of glucose is compatible with the observed less tight binding of D-glucal to the oxidized form of the enzyme (Rogers & Brandt, 1971*a*).

The inhibitory effect of halide ions (Bright & Appleby, 1969, Rogers & Brandt, 1971*b*,*c*) seems to be compatible with the assumption of an interaction of the halide ion with His516. In the present model, His516 $N^{\delta1}$ is hydrogen bonded to the water molecule W109, which could be replaced by a halide ion as shown by force-field calculations (Fig. 7). This would stabilize a positively charged doubly protonated His516 and, depending on pH, would thus inhibit the proton-abstraction step required prior to hydride transfer.

3.3.3. Complexes with other sugars. GOX exhibits at least a 20-fold higher affinity and a fivefold higher turnover rate (k_{cat}) for β-D-glucose than for other monosaccharides (Pazur & Kleppe, 1964). The binding of the substrate is thought to be the rate-limiting step in the GOX reaction (Bright & Appleby, 1969). Simulation of the Michaelis-type complexes for other hexopyranoses using the molecular-mechanics method shows that the favourable contact distances observed for β-D-glucose are not possible for the other sugars. In the case of β-D-glucose, which cannot be oxidized by GOX unless it is mutarotated to the β-anomer (Adams *et al.*, 1960), seven hydrogen bonds are formed to protein residues, as well as four hydrogen bonds to water molecules and one intramolecular hydrogen bond. Most of these bonds are at less favourable angles and distances compared with the β-anomer. The most significant change in the β-D-glucose complex, however, is an increase in the distance between H(O1) and N of

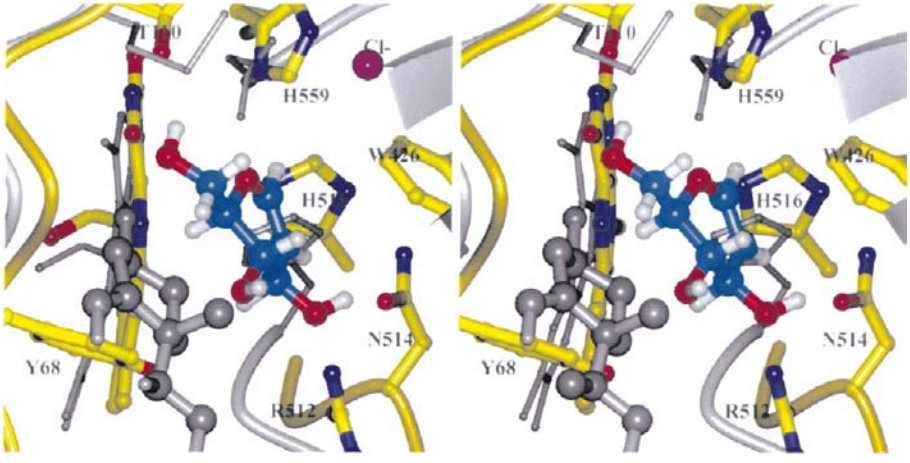

Figure 7
Stereoview of the active site of glucose oxidase from *A. niger* with the modelled inhibitors D-glucal and chloride, drawn with *MOLSCRIPT* (Kraulis, 1991) and rendered with *gl_render* (Esser & Deisenhofer, unpublished program) and *POV-Ray*. For comparison, selected residues in the active site of the experimental substrate analogue complex of cholesterol oxidase (Li *et al.*, 1993) are superimposed in grey. For D-glucal, C atoms are coloured cyan, H atoms white and the Cl ion magenta.

His516 to 2.0 Å and between H(C1) and N5 of FAD to 2.7 Å as a consequence of the interchange of the hydroxyl group and the H atom at C1.

The complex with β-2-deoxyglucose is very similar to that with β-D-glucose, with only the hydrogen bond to the Asn514 backbone O atom missing. Accordingly, although 2-deoxy-D-glucose is oxidized at a tenfold lower rate than β-D-glucose, the binding constant for 2-deoxy-D-glucose is very similar to that for β-D-glucose (Nakamura & Ogura, 1968).

For D-mannose, GOX has a 400-fold lower specificity constant than for β-D-glucose (Gibson *et al.*, 1964). In the β-D-mannose complex, the hydrogen bond from β-D-glucose to the backbone O atom of Asn514 is instead formed to the Asn514 side-chain O1, and an additional unfavourable contact is formed between the axial O2 hydroxyl group and Trp426. These interactions force the mannose to a position where the remaining hydrogen-bond distances and angles are less favourable compared with β-D-glucose.

D-Galactose is an extremely poor substrate for GOX, with a 1000-fold lower specificity constant than β-D-glucose (Gibson *et al.*, 1964). In comparison with β-D-glucose, the axial O4 group of β-D-galactose has lost the hydrogen bonds to Tyr68 and Arg512. A new hydrogen bond to a water molecule is formed and an unfavourable contact to the Trp426 side chain exists.

D-Xylose, which lacks the exocyclic CH_2OH-group, is another poor substrate for GOX, with a 3000-fold lower specificity constant than β-D-glucose (Gibson *et al.*, 1964). In comparison with β-D-glucose, three weaker hydrogen bonds to Thr110, FAD O4 and to a water molecule are missing in the complex with β-D-xylose. This leads to a configuration of the sugar with a less favourable angle between HC1 and the FAD N5, and its O1 group is only poorly stabilized by His559, which is directed towards the FAD O4.

From the present model it remains unclear how the two exchanges in the active sites of asp-gox and pen-gox, Thr/Ser110 and Tyr/Trp515, could effect the sixfold higher affinity and tenfold higher specificity constant, k_{cat}/K_m, for β-D-glucose observed for the enzyme from *P. amagasakiense* (Kalisz *et al.*, 1997). The simulations of the enzyme–substrate complexes and the results of the site-directed mutagenesis experiments are, however, compatible with the proposed position of the substrate, which indicates the involvement of Tyr68, Thr/Ser110, Arg512, Asn514 and His559 in substrate binding, and provide explanations for the lower affinity of GOX to other hexopyranoses, for the possible mechanism of inhibition by D-glucal and for the lack of product inhibition by D-gluconolactone.

References

Adams, E. C. Jr., Mast, R. L. & Free, A. H. (1960). *Arch. Biochem. Biophys.* **91**, 230–234.

Alvarez-Icaza, M., Kalisz, H. M., Hecht, H.-J., Aumann, K. D., Schomburg, D. & Schmid, R. D. (1995). *Biosens. Bioelectr.* **10**, 735–742.

Bayly, C. I., Cieplak, P., Cornell, W. D. & Kollman, P. A. (1993). *J. Phys. Chem.* **97**, 10269–10280.

Becke, A. D. (1993). *J. Chem. Phys.* **98**, 5648–5652.

Bright, H. J. & Appleby, M. (1969). *J. Biol. Chem.* **244**, 3625–3634.

Bright, H. J. & Porter, D. J. T. (1975). *The Enzymes*, 3rd ed., edited by P. D. Boyer, Vol. 12, pp. 421–505. New York: Academic Press.

Brünger, A. T., Kuriyan, J. & Karplus, M. (1987). *Science*, **235**, 458–460.

Cavener, D. R. (1992). *J. Mol. Biol.* **223**, 811–814.

Collaborative Computational Project, Number 4 (1994). *Acta Cryst.* D**50**, 760–763.

Cornell, W. D., Cieplak, P., Bayly, C. I., Gould, I. R., Merz, K. M., Ferguson, D. M., Spellmeyer, D. C., Fox, T., Caldwell, J. W. & Kollman, P. A. (1995). *J. Am. Chem. Soc.* **117**, 5179–5197.

Cornell, W. D., Cieplak, P., Bayly, C. I. & Kollman, P. A. (1993). *J. Am. Chem. Soc.* **115**, 9620–9631.

Esnouf, R. M. (1997) *J. Mol. Graph.* **15**, 132–134.

Fitzgerald, P. M. D. (1988). *J. Appl. Cryst.* **21**, 273–278.

Frisch, M. J., Trucks, G. W., Schlegel, H. B., Gill, P. M. W., Johnson, B. G., Robb, M. A., Cheeseman, J. R., Keith, T., Petersson, G. A., Montgomery, J. A., Raghavachari, K., Al-Laham, M. A., Zakrzewski, V. G., Ortiz, J. V., Foresman, J. B., Peng, C. Y., Ayala, P. Y., Chen, W., Wong, M. W., Andres, J. L., Replogle, E. S., Gomperts, R., Martin, R. L., Fox, D. J., Binkley, J. S., Defrees, D. J., Baker J., Stewart, J. P., Head-Gordon, M., Gonzalez, C. & Pople, J. A. (1995). *GAUSSIAN* 94, revision B3. Gaussian, Inc., Pittsburgh, PA, USA.

Gibson, Q. H., Swoboda, B. E. P. & Massey, V. (1964). *J. Biol. Chem.* **237**, 3927–3934.

Hariharan, P. C. & Pople, J. A. (1973). *Theor. Chim. Acta*, **28**, 213–222.

Hecht, H.-J., Kalisz, H. M., Hendle, J., Schmid, R. D. & Schomburg, D. (1993). *J. Mol. Biol.* **229**, 153–172.

Hehre, W. J., Ditchfield, R. & Pople, J. A. (1972). *J. Chem. Phys.* **56**, 2257–2261.

Hendle, J., Hecht, H.-J., Kalisz, H. M., Schmid, R. D. & Schomburg, D. (1992). *J. Mol. Biol.* **223**, 1167–1169.

Jones, T. A. (1985). *Methods Enzymol.* **115**, 157–171.

Jones, T. A, Zou, J. Y., Cowan, S. W. & Kjeldgaard, M. (1991). *Acta Cryst.* A**47**, 110–119.

Jorgensen, W. L., Chandrasekhar, J., Madura, J. D., Impey, R. & Klein, M. (1983). *J. Chem. Phys.* **79**, 926–935.

Kalisz, H. M., Hecht, H.-J., Schomburg, D. & Schmid, R. D. (1990). *J. Mol. Biol.* **213**, 207–209.

Kalisz, H. M., Hecht, H.-J., Schomburg, D. & Schmid, R. D. (1991). *Biochem. Biophys. Acta*, **1080**, 138–142.

Kalisz, H. M., Hendle, J. & Schmid, R. D. (1997). *Appl. Microbiol. Biotechnol.* **47**, 502–507.

Kiess, M., Hecht, H.-J. & Kalisz, H. M. (1998). *Eur. J. Biochem.* **252**, 90–99.

Kraulis, P. J. (1991). *J. Appl. Cryst.* **24**, 946–950.

Laskowski, R. A., MacArthur, M. W., Moss, D. S. & Thornton, J. M. (1993). *J. Appl. Cryst.* **26**, 283–291.

Lee, C., Yang, G. & Parr, R. G. (1988). *Phys. Rev. B*, **37**, 785–789.

Li, J., Vrielink, A., Brick, P. & Blow, D. M. (1993). *Biochemistry*, **32**, 11507–11515.

McRee, D. E. (1993). *Practical Protein Crystallography.* London: Academic Pres.

Nakamura, S. & Ogura, Y. (1968). *J. Biochem.* **63**, 308–316.

Nicholls, A. J. (1993). *GRASP: Graphical Representation and Analysis of Surface Properties.* Columbia University, NY, USA.

Otwinowski, Z. & Minor, W. (1996). *Methods Enzymol.* **276**, 307–326.

Pazur, J. H. & Kleppe, K. (1964). *Biochemistry*, **3**, 578–583.

Pearlman, D. A., Case, D. A., Caldwell, J. C., Seibel, G. L., Singh, U. C., Weiner, P. & Kollman, P. A. (1991). *AMBER* 4.0, University of California, San Francisco, USA.

Rogers, M. J. & Brandt, K. G. (1971*a*). *Biochemistry*, **10**, 4624–4630.

Rogers, M. J. & Brandt, K. G. (1971*b*). *Biochemistry*, **10**, 4630–4635.

Rogers, M. J. & Brandt, K. G. (1971*c*). *Biochemistry*, **10**, 4636–4641.

Ryckaert, J. P., Cicotti, G. & Berendsen, H. J. C. (1977). *J. Comput. Phys.* **23** 327–341.
Sanner, C., Macheroux, P., Rüterjans, H., Müller, F. & Bacher, A. (1991). *Eur. J. Biochem.* **196**, 663–672.
Schomburg, D. & Reichelt, J. (1988). *J. Mol. Graph.* **6**, 161–165.
Voet, J. G., Coe J., Epstein, J., Matossian, T. & Shipley, T. (1981). *Biochemistry*, **20**, 7182–7185.
Vrielink, A., Lloyd, L. F. & Blow, D. M. (1991). *J. Mol. Biol.* **219**, 233–254.
Wallace, A. C., Laskowski, R. A. & Thornton, J. M. (1995). *Protein Eng.* **8**, 127–134.
Wilson, R. & Turner, A. P. F. (1992). *Biosens. Bioelectr.* **7**, 165–185.
Witt, S. (1996). PhD thesis. University of Hanover, Germany.